Available online at www.sciencedirect.com
SCIENCE DIRECT®
Journal of Applied Geophysics xx (2006) xxx – xxx
JOURNAL OF APPLIED GEOPHYSICS
www.elsevier.com/locate/jappgeo

Ground Penetrating Radar imaging of two large sand blow craters related to the 2001 Bhuj earthquake, Kachchh, Western India

D.M. Maurya [a], B. Goyal [a], A.K. Patidar [a], N. Mulchandani [a], M.G. Thakkar [b], L.S. Chamyal [a,*]

[a] Department of Geology, M. S. University of Baroda, Vadodara-390 002, India
[b] Department of Geology, R. R. Lalan Science College, Bhuj, Kachchh-370 001, India

Received 19 July 2004; accepted 13 February 2006

Abstract

The 2001 Bhuj earthquake (Mw 7.7) formed several medium to large sand blow craters due to extensive liquefaction of the sediments comprising the Banni plain and Great Rann of Kachchh. We investigated two large closely spaced sand blow craters of different morphologies using Ground Penetrating Radar (GPR) with a view to understand the subsurface deformation, identify the vents and source of the vented sediments. The study comprises velocity surveys, GPR surveys using 200 MHz antennae along three selected transects that is supplemented by data from two trenches excavated. The GPR was able to provide good data on stratigraphy and deformation up to a depth of 6.5 m with good resolution. The GPR successfully imaged the subsurface characteristics of the craters based on the contrasting lithologies of the host sediments and the sediments emplaced in the craters. The GPR also detected three vertical vents of ~1 m width continuing throughout the profile which are reflected as high amplitude vertical events. We conclude that the large sand blows during the 2001 Bhuj earthquake were produced due to liquefaction of sediments in the subsurface at >6.5 m depth and that the clay-rich sediments of the Banni plain have behaved as the fine grained cap over it. The present study provides a modern analogue for comparing the liquefaction features of past great earthquakes (for example, the 1819 earthquake) that have occurred in the Kachchh region to understand the phenomena of liquefaction.

Keywords: Ground Penetrating Radar (GPR); Liquefaction; Sand blow crater; 2001 Bhuj earthquake; Kachchh

1. Introduction

Ground Penetrating Radar (GPR) is now a well established geophysical technique for high resolution imaging of the geological features in the shallow subsurface (Jol and Bristow, 2003). The usefulness of GPR in the fields of stratigraphy, sedimentology, neotectonics and palaeoseismology has already been demonstrated (Bridge et al., 1998; Feilding et al., 1999; Busby and Merritt, 1999; Bano et al., 2000; Chow et al., 2001; Lui and Li, 2001; Neal, 2004; Maurya et al., 2005). However, the application of GPR in the study of earthquake induced liquefaction features is still in its infancy. The problem in such studies is twofold. One is the highly variable morphological forms that the earthquake induced liquefaction features can assume (Sims and Garvin, 1995). Secondly, application of GPR in identifying and characterizing these features in diverse lithologic settings is yet to be

* Corresponding author.
E-mail address: lschamyal@yahoo.com (L.S. Chamyal).

0926-9851/$ - see front matter © 2006 Elsevier B.V. All rights reserved.
doi:10.1016/j.jappgeo.2006.02.001

demonstrated, as these features are strongly dependent on local geologic set up (Obermeier, 1996). Moreover, no GPR based study has been carried out so far on the liquefaction features produced by contemporary earthquakes.

Large sand blows are one of the spectacular surface features formed due to seismically induced liquefaction. Most documented high magnitude earthquakes have produced large sand blows, however, their manifestations have been varied and heavily dependent on local geologic and geographic setting. However, deformation effects of liquefaction in vertical section have rarely been documented. Such studies are important from the point of view of understanding the intricacies of internal and external geometry of the liquefaction features, which can be used for precise identification and characterization of the similar features produced by ancient earthquakes whose precise locations and characteristics beyond trenching depths are often unknown. Here we present the results of the GPR study of the largest documented sand blow crater located about 45 km northwest of the epicenter near Umedpar (Tuttle et al., 2002) and formed in clay-rich sediments of the Banni plain (Fig. 1) during the devastating Bhuj earthquake of 26th January 2001. The study was aimed at understanding the internal structure of the sand blow crater in the shallow subsurface and if possible, identify the source horizon of liquefied sand ejected on the surface. The study intends to demonstrate the applicability of GPR in investigating large liquefaction features and provide a modern analogue for comparing similar features produced by past earthquakes.

2. The Banni plain and 2001 Bhuj earthquake

The flat terrain of Banni plain and the Great Rann (Fig. 1) together comprise a vast barren landscape that is hostile and almost unnavigable (Glennie and Evans, 1976). These contiguous terrains occur a few meters above sea level and are believed to be part of a former gulf occupying an E–W trending tectonic depression. The Banni plain is considered to be a vast raised mudflat (Kar, 1995) while the Great Rann resembles a salt marsh (Glennie and Evans, 1976). The Great Rann gets submerged by storm tides from the west and monsoon rains, while the Banni plain is only flooded by rivers from the south and monsoon precipitation (Glennie and Evans, 1976). Owing to its unique geographic and geologic setting, the area is characterized by a shallow water table. During monsoon, the water table in the Banni plain is almost at the surface, which, descends down by few meters during the dry summer season when the temperatures constantly hover around 45 °C and even above. The area has been repeatedly affected by large-scale liquefaction due to several large

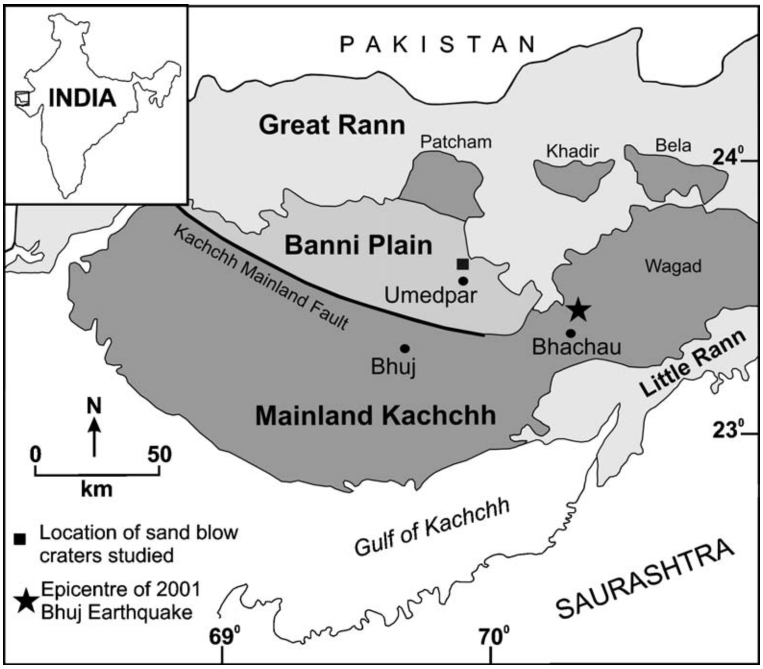

Fig. 1. Map of Kachchh region showing location of the sand blow craters studied. Inset—location map.

magnitude earthquakes in the historic past (Quittmeyer and Jacob, 1979).

The Bhuj earthquake (Mw 7.7) occurred on 26th January 2001 whose epicenter was located at 23°36′ N latitude and 70°34′ E longitude. The earthquake received immediate attention of the earth scientists as it offered 'first-of-a-kind laboratory' for the study of large magnitude intra-plate earthquakes (Schweig et al., 2003). The earthquake induced large-scale surface deformation in the form of lateral spreads, extensional cracks, monoclinal flexures, tear faults and widespread liquefaction (Rajendran et al., 2001, 2002; Tuttle et al., 2002; McCalpin and Thakkar, 2003). A significant feature of this earthquake was the large-scale liquefaction covering an area of more than 15,000 km^2 (Rajendran et al., 2001, 2002; Tuttle et al., 2002). The Banni plain witnessed huge outpourings of water and sediment onto the surface which vented out from fissures or vents aligned mostly along east west direction (Rajendran et al., 2001). Some heterogeneities in the distribution of the liquefaction features have been documented (Tuttle et al., 2002; Thakkar and Goyal, 2004), which are yet awaiting a satisfactory explanation. These concern mainly with the pattern of distribution of the liquefaction features with respect to the epicenter and the source of the sediments vented on the surface. Lithologically, the sediments of the Banni Plain and Great Rann (host sediments) are known to comprise fine grained sands, silts and clays deposited in an embayed gulf during the Holocene which now occur ∼4 m above mean sea level (Srivastava, 1971; Roy and Merh, 1981; Kar, 1995). However, no detailed stratigraphic studies on these sediments are available that could serve as a basis for understanding the widespread liquefaction produced during the 2001 Bhuj earthquake.

3. Morphology of the sand blow craters

The area of Banni plain, to the north of Umedpar, was severely affected by the venting of huge amounts of water and sand, which left behind several medium to large sized sand blow craters (Rajendran et al., 2001). We selected a 'couplet' of two large sand blows (Fig. 2a, b), one of them identified as the largest sand blow crater (Tuttle et al., 2002), for our investigations. The craters continued to spout saline water and sediments even 3 weeks after the earthquake (Rajendran et al., 2001) and remained filled with muddy water, at least, for a year. However, their present morphology has been partially modified (Fig. 2b) since the time of their formation due to combined effect of collapse of the margins and sediments washed into the depression during subsequent monsoons. The craters were dry at the time of our study and shared a partially collapsed common rim at their junction which occurred at a lower level than the outer rim at the ground level (Fig. 2b). The crater to the west (Crater-I) shows an oblong shape with the longer axis along the NNW–SSE direction and is reportedly, the largest crater produced during the 2001 Bhuj earthquake (Tuttle et al., 2002). The crater possessed a maximum length of 10 m and a width of 5 m along the NNE–SSW direction. The one to the east (Crater-II) showed a circular outline with a diameter of 8 m and maximum depth of 76 cm at the center. Outside the craters, an apron of coarse sand occurs, presumably representing the sediment vented out of the craters. The apron of vented sand is recorded as 33 m long, 32 m wide and 26 cm thick (Tuttle et al., 2002).

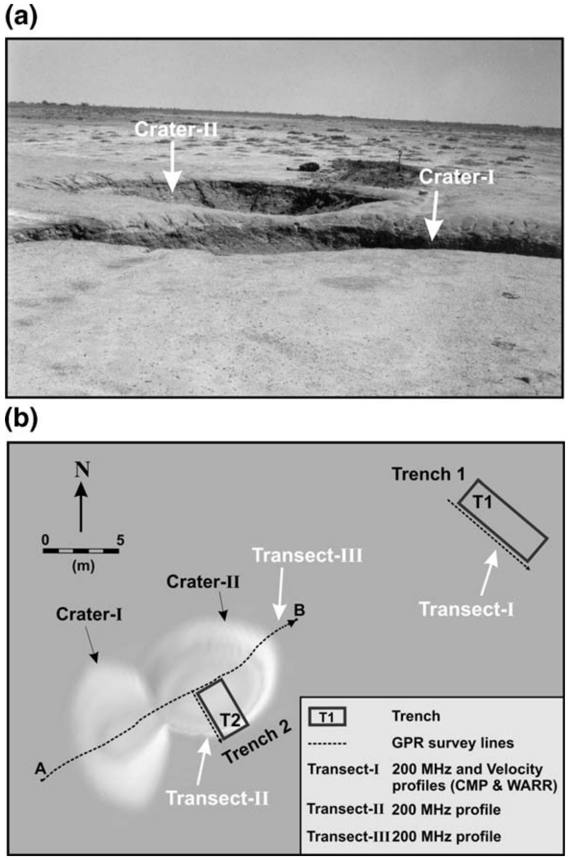

Fig. 2. (a) Northeast facing view of the craters studied. The craters remained filled with water for about a year after the earthquake. The above photograph was taken in December 2002, when the craters had dried out. Note the vegetation-free barren landscape of the Banni plain in the background. (b) Three-dimensional model of the site and the sand blow craters as they appeared at the time of GPR studies during March 2004. Location of GPR transects and the trenches is also shown.

4. GPR investigations

GPR technique involves transmission of high frequency electromagnetic waves into the ground which is reflected back from the sediment interfaces showing variable electrical properties in the subsurface and is received on the surface and is displayed in the form of a profile (Davis and Annan, 1989) showing horizontal survey distance versus vertical two-way travel time in nanoseconds (1 ns $=10^{-9}$ s). The properties which govern the passage of electromagnetic waves in the subsurface are dielectric permittivity and electrical conductivity (Davis and Annan, 1989). The clayey sediments are normally known to show higher attenuation of radar signal, especially of higher frequencies, thereby affecting penetration as they possess high water retention capacity and low electrical resistivity (Jol et al., 1996). However, recent studies have observed increased permittivity in clayey sediments showing variations in grain size, water content and salt contents, which results in high dielectric contrast between clay and sand layers enabling detection of sand–clay interfaces (Saarenketo, 1998; Lui and Li, 2001; Carreon-Freyre et al., 2003). Small-scale textural changes in sediments also result in changes in permittivity that are sufficient to cause reflection of radar signals (Van Dam and Schlager, 2000).

We carried out GPR studies using a SIR-20 system manufactured by Geophysical Survey Systems Inc. Keeping in view, the lack of knowledge on subsurface stratigraphy and expected presence of clayey sediments, we excavated two trenches to support our interpretation of GPR data. We also resorted to increased transmitter power as it is known to increase the depth of penetration and improve the continuity of reflectors with little effect on resolution (Jol, 1995). Location of GPR transects and trenches are shown in Fig. 2b. Three transects were selected for the present study (Transect-I, -II and -III). The velocity surveys (CMP and WARR) were carried out along the NW–SE trending Transect-I located ~26 m to the NE of the craters. Same transect was used for GPR profiling by 200 MHz monostatic shielded antennae followed by trenching (Trench-1) to confirm the velocity data and to correlate the reflected patterns of radar waves with subsurface lithological variations at the site. This was necessary, as no stratigraphic details are known for the sediments of the Banni plain and Great Rann. Transect-II comprises the SE margin of Crater-II. GPR profiling and trenching were carried out along this transect for delineating the crater margin and internal structure of the crater sediments. Early reports of the liquefaction during Bhuj earthquake had pointed out E–W direction as the preferred orientation of the sand blows and fissures (Rajendran et al., 2002). We, therefore, selected a NE–SW transect (Transect-III) passing through both the craters (Fig. 2b) for the GPR survey, assuming the presence of maximum number of vents, if any, along this trend. The ground truth for this transect is provided by the northwestern wall of the trench along Transect-II. All the 200 MHz profiles were obtained by manually towing the antennae along the selected transects. Several sample profiles were collected along each transect to obtain the best ‘trade off’ between resolution and depth. The best profiles were selected for post-survey data processing and interpretation.

As the site of study was totally devoid of vegetation and civilisation structures (Fig. 2a), good quality data were obtained up to a depth of 6.5 m. None of the profiles showed diffraction patterns in the form of hyperbolic reflections, characteristic of such extraneous objects. In view of this, the processing of the profiles was kept to the minimum so as to avoid obliteration of original data and introduction of artifacts. Post-survey data processing included Distance Normalization to equalise the scanning speed. Combinations of various filters (vertical and horizontal) were used to cut out the frequencies above an established threshold. The auto gain function (AGC) with 5 points was applied to enhance the data quality and emphasize the low amplitude sections. The GPR data along Transect-III were Surface Normalized to remove the topographic effects and reorient the deeper reflectors at their true positions.

5. Velocity analysis and lithological characterization (Transect-I)

The CMP (Common midpoint) and WARR (wide angle reflection refraction) gathers were obtained along Transect-I located on the flat ground adjacent to the craters so as to encounter the undeformed sediments of the area in their true position. The profiles were obtained using MLF (Multi-low Frequency) antennae set at 80 MHz center frequency and 1 m minimum offset distance between transmitter and receiver. In CMP profiling, each transmitter and receiver antenna was moved away from mid-point with 15 cm step size. For WARR profiling, the transmitter was fixed and receiver was shifted between measured points with 15 cm step size. The value of 50 stacks/scan was set to decrease signal-to-noise ratio. The velocity was determined by running the velocity analysis programme using RADAN

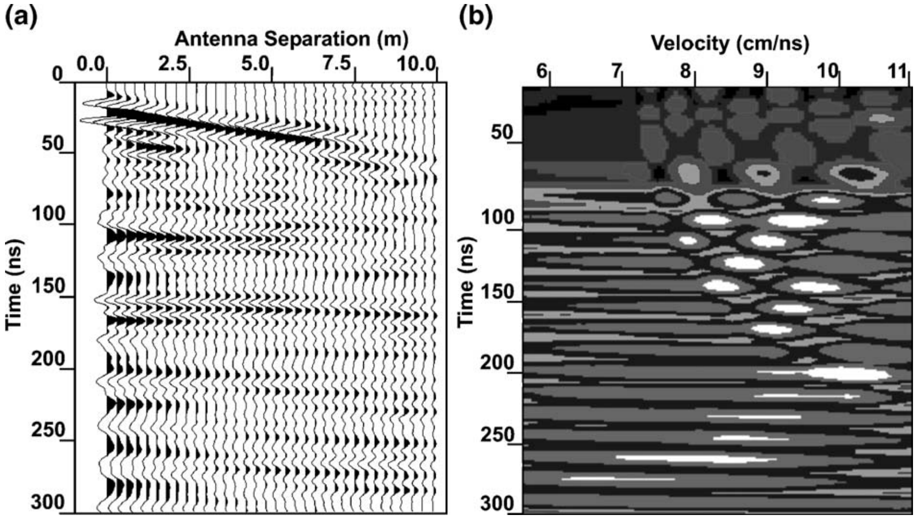

Fig. 3. CMP data obtained along Transect-I (a) and the corresponding velocity diagram (b).

software. Both, the CMP and WARR profiles yielded similar results, which were averaged to determine the velocity for time/depth conversion. The calculated average velocity obtained is 0.0896 m/ns, which yields a dielectric constant (E_r) of about 11.20 for the site under study. One of the CMP profiles and velocity diagram is shown in Fig. 3a, b.

The velocity surveys along Transect-I was followed by GPR profiling with 200 MHz antennae and trenching to characterize the subsurface lithological variations and related radar signatures/facies. We identified distinct groups of radar reflections or facies on the basis of well-defined coherent radar reflections with lateral continuity and correlating them with the vertical lithological variations in the trench wall. The trench, 6 m long, 2 m wide and 2.1 m deep, was excavated exactly along the survey line. The trench revealed a horizontally stratified three layered clay-rich sediment succession shown in Fig. 4. At base of the trench, alternations of 5–10 cm thick strata of fine sand and clay were encountered that continued upward up to 1.3 m depth. Overlying this is a 0.9 m thick horizon of finely laminated clay followed

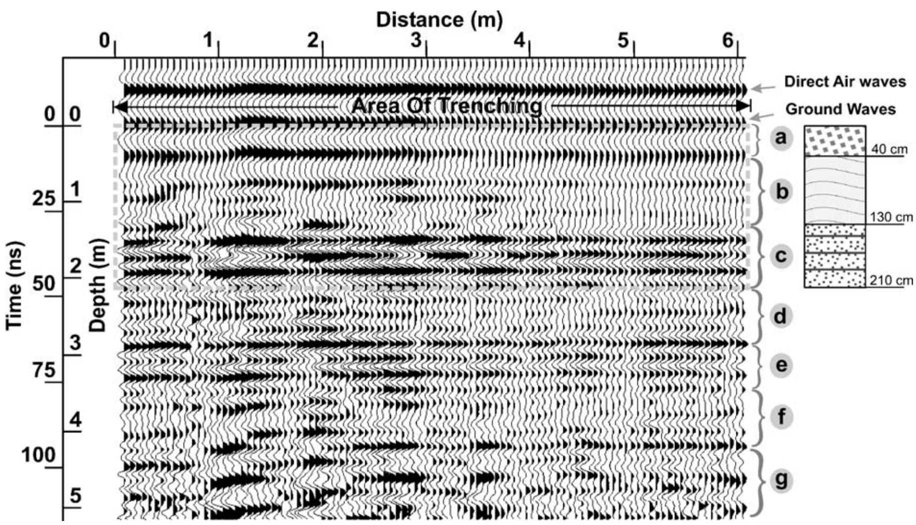

Fig. 4. GPR profile (time-zero corrected) obtained along Transect-I using 200 MHz antennae and vertical lithology of the trench along the same transect. Note the distinct groups of radar reflections corresponding to lithological variations in the trench. Based on the correlation of reflections with the lithology of the trench, the lithologies beyond trench depth have also been interpreted. (a) Silty clay, (b) finely laminated clay, (c) sand clay alternations, (d) laminated clay, (e) sand clay alternations, (f) laminated clay, (g) sand clay alternations (possibly thicker layers).

upward by 0.4 m thick silty clay. The succession is covered by a thin veneer of medium coarse sand ejected form the nearby crater during the earthquake. The sediments showed mild deformation in the form of small-scale gentle flexures and a microfault within the laminated clay. Low water table conditions at the time of our study are attested by the fact that water did not enter the trench even after 10 days.

Reflection patterns of radar waves are related to lithologic and stratigraphic characteristics of sediments, which can be used to subdivide GPR profiles into radar stratigraphic units (radar facies) that can be related to broadly uniform lithologies (Jol and Smith, 1991; Gawthrope et al., 1993; Jol and Bristow, 2003). Interpretation of GPR profiles involves picking up major reflections, reflection terminations followed by characterizing these in terms of sedimentary and deformation features which forms the basis for reconstructing a relative chronology of sedimentary deposits (Jol and Bristow, 2003). The 200 MHz profile (Fig. 4) shows three prominent sets of reflectors (radar facies) that correspond with the three layered sediment succession encountered in the trench. The reflector at 0.4 m (~10 ns) correlates with the silty clay sediments marking the top of the succession in the trench. The underlying radar facies, from 0.4 m to 1.3 m (~10 ns to ~32 ns), comprise largely homogenous low amplitude reflections which are related to the finely laminated clays. The alternations of fine sand and clay are represented by a distinct radar facies consisting of closely spaced parallel reflectors up to ~46 ns. Further downward, the radar facies are repeated, which suggests repetition of lithologies and clay-rich sediments in general. The profile shows the suitability of the Banni plain sediments for GPR investigations. The sediments, though, clay-rich, show vertical heterogeneity in terms of grain size, which in turn determines the moisture retention capacity. The variations allow for detection of lithologies as distinct groups of reflections of radar facies. The GPR, however, failed to detect the mild deformation seen in the trench sediments. The profile shows no signature of water table, suggesting that the depth of the water table was greater than 5 m at the time of survey.

6. Radar characteristics of the sand blow craters

We studied the craters along two transects. The SW margin (Transect-II) of the circular crater (Crater-II) was studied to image the crater margin and the sediments within the crater and those outside it (Fig. 2b). The GPR data are correlated with the trench excavated along this transect. Transect-III is oriented NE–SW and passes through both the craters. This transect was aimed at obtaining composite data on both craters and detecting the vents and the source horizon of the sediments ejected on the surface.

6.1. Transect-II

GPR profiling by 200 MHz antennae preceded the excavation of the trench along Transect-II. A 2.2 m deep trench was excavated along this transect. This was done to characterize the margin of the crater and the internal structure of the crater with a view to correlate the profile obtained across the craters. The floor of the crater was made horizontal before the GPR survey so as to avoid topographic correction during post-survey processing. Fig. 5 shows GPR data and log of the trench along Transect-II. A sharp contrast in the sediment characteristics is observed between the sediments within the crater and outside the crater (host sediments). The sediment succession outside the crater (Fig. 5b) is similar to the three-layered sediment succession encountered in the trench along Transect-I (Fig. 4).

Within the craters, the sediments encountered are different from the host sediments. The sediments inside the crater comprise clay and sand ejected from the subsurface, which show a sharp contact with the host sediments. We confirmed the velocity of the radar waves by inserting a metallic pipe in the crater sediments exposed in the trench wall and running a profile with 200 MHz antennae over it. The metal pipe was placed on 1.35 m from the surface which was picked by radar near 31 ns (after time zero correction). We therefore used the same value for interpreting the GPR data of the crater. The dominant lithology encountered within the crater and exposed in the trench wall includes wet, sticky, plastic, structureless, greenish black clay that is thickest at the center of the crater and tapers towards the margin. Within this clay, thin layers of liquefied sand are seen (Fig. 5b) The crater sediments underlying the clay comprise sediments with varying proportions of clay, silty clay and large clasts of finely laminated medium to coarse sand. The laminations within the sand clasts dip towards the center of the crater (Fig. 5b). The entire succession of crater sediments is capped by a 0.5 m thick structureless silty sand at the top, which constitutes the post-earthquake fill material derived from the area around the craters and deposited within the crater depression. The trench data show that the GPR accurately imaged the crater margin and the finer lithological variations of the crater sediments (Fig. 5a, b). The host sediments are characterized by persistent,

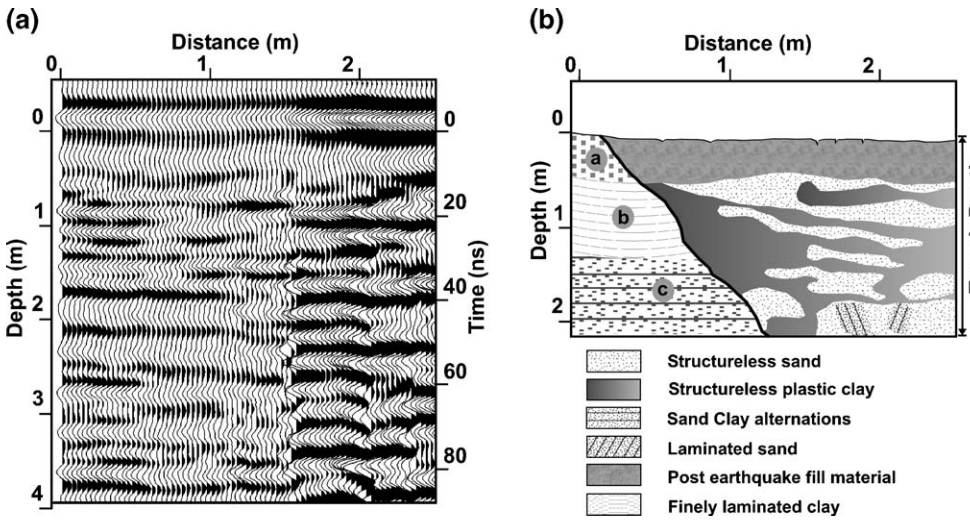

Fig. 5. (a) 200 MHz GPR profile (time-zero corrected) across the SW margin (Transect-II) of Crater-II. (b) Simplified log of the trench along Transect-II. Note the contrast between the sediments outside the crater (host sediments) and sediments within the crater. The stratigraphy of the host sediments and their radar reflections are similar to those in Fig. 4.

parallel, consistent, continuous and planar reflections (Fig. 5a) that are similar to the GPR data along Transect-I. The radar facies of the crater sediments is characterized by group of discontinuous reflectors that show several abrupt truncations (Fig. 5a). The wet, plastic clay is marked by homogenous and distinctive radar signatures. The sand–clay interfaces are characterized by high amplitude strength. Beyond trench depth, the profile shows narrowing of the crater into a vent through which sediments traveled upward from deeper levels. The radar data suggest that the vent is filled dominantly by structureless sand with little amount of clay.

6.2. Transect-III

The GPR profile of the craters (Transect-III) shows lithology, internal geometry and deformation of the sediment up to a depth of 6.5 m (Fig. 6a). Apart from the identification of stratigraphic heterogeneities, internal geometry and deformation of the sediments within the sand blow crater, the GPR has also been successful in the detection of vents that were responsible for ejection of water and liquefied sand onto the surface. The profile is vertically divisible into groups of similar reflectors, which are associated with the lithological variations down the craters.

The profile shows a sharp contact between the layered host sediments and the crater sediments. The two craters are clearly discernible in the profile. Though the craters occur very close to each other, both the craters have maintained their individual fidelity and are of non-coalescing type. The northwestern wall of the trench along Transect-II coincides with the GPR survey line of Transect-III (Fig. 2b). The lithological composition of the crater sediments observed in the northwestern wall (Fig. 6b) is comparable to that seen in the southwestern wall of the trench shown in Fig. 5b. Thin layers of liquefied sand within the greenish black structureless clay show convolutions (Fig. 6c). The lithology below the clay is dominated by sand, which includes structureless sand and large clasts of laminated sand. The laminations dip towards the center of the crater (Fig. 6b, c) suggesting the presence of a sand vent below. Fig. 6a shows that the trench section is located over one of the vents (V2). Three non-intersecting vertical vents associated with the craters and filled with liquefied sand have been detected (Fig. 6a). The sand vents are detected as persistent high amplitude vertical events at the central part of the craters (Fig. 7). The eastern circular crater (Crater-II) shows two vents which maintain a separation distance of 2 m down the profile throughout the achieved depth. One of the vents is located at the center of the crater while the other is located on its eastern side. Both vents show identical widths of ~1 m. The western elongated crater (Crater-I) shows a single vertical vent at center. The dimensions of this vent appear to be >1 m. The vents are normally filled by liquefied sand, clay, sand–clay clasts and fragments of host sediments eroded from the side walls, as the subsurface material travel upward under pressure, during the formation of the sand blow (Sims and Garvin, 1995; Obermeier, 1996). We believe that the width of

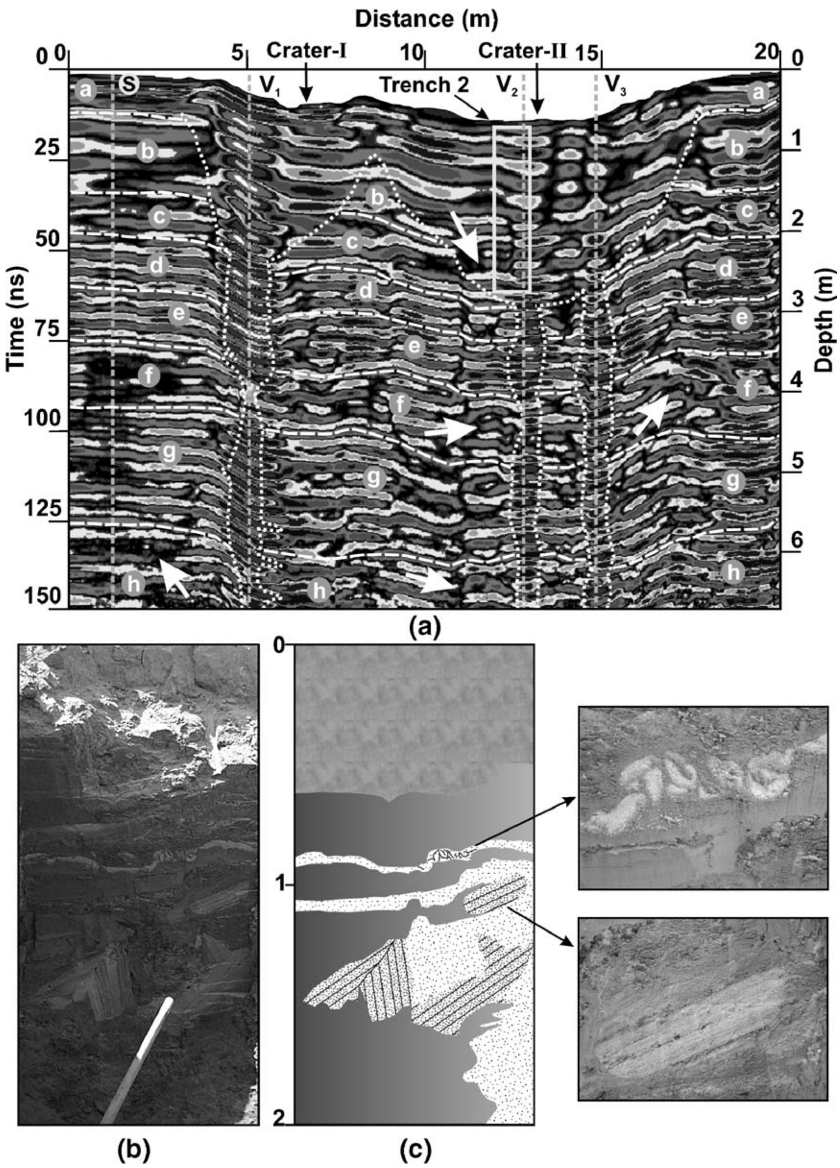

Fig. 6. (a) Interpreted GPR profile of the sand blow craters along Transect-III showing the inferred morphology of the craters, internal deformation and the sand vents. The profile has been interpreted on the basis of radar reflection patterns observed along the Transects-I and -II. Note the distinct reflections of the crater sediments and the layered host sediments. The notations in panels (a–g) have the same meaning as mentioned in Fig. 4; (h) laminated clay. Enclosed area marks the position of the northwestern wall of the trench excavated along Transect-II. Arrows indicate the areas of plastic deformation. The vents are indicated as V_1, V_2 and V_3. Vertical dashed lines (S, V_1, V_2 and V_3) represent the locations of the traces shown in Fig. 7. (b) View of the northwestern wall of the trench along Transect-II. Note the structureless clay and sands with large clasts of laminated sand constituting the crater sediments. (c) Tracing overlay of trench section highlighting the lithological variations with close view of the convolutions and laminated sand. Legend is same as given in Fig. 5b.

the vents detected by the GPR data includes the composite lithology of the vents as mentioned above. The varying widths of the vents in the subsurface can be attributed to differential erosion of the host sediments depending on the cohesive strength of the stratigraphic layers during the upward movement of sand and water (Sims and Garvin, 1995). The consistent presence of vents down the profile (Fig. 6a) suggests that the source horizon of the liquefied sand vented is located still deeper in the subsurface.

The host sediments are distinctly identifiable on the basis of their layered appearance and the similarity of reflections with the profiles along Transects-I and -II. Beneath the craters, the host sediments show a gentle

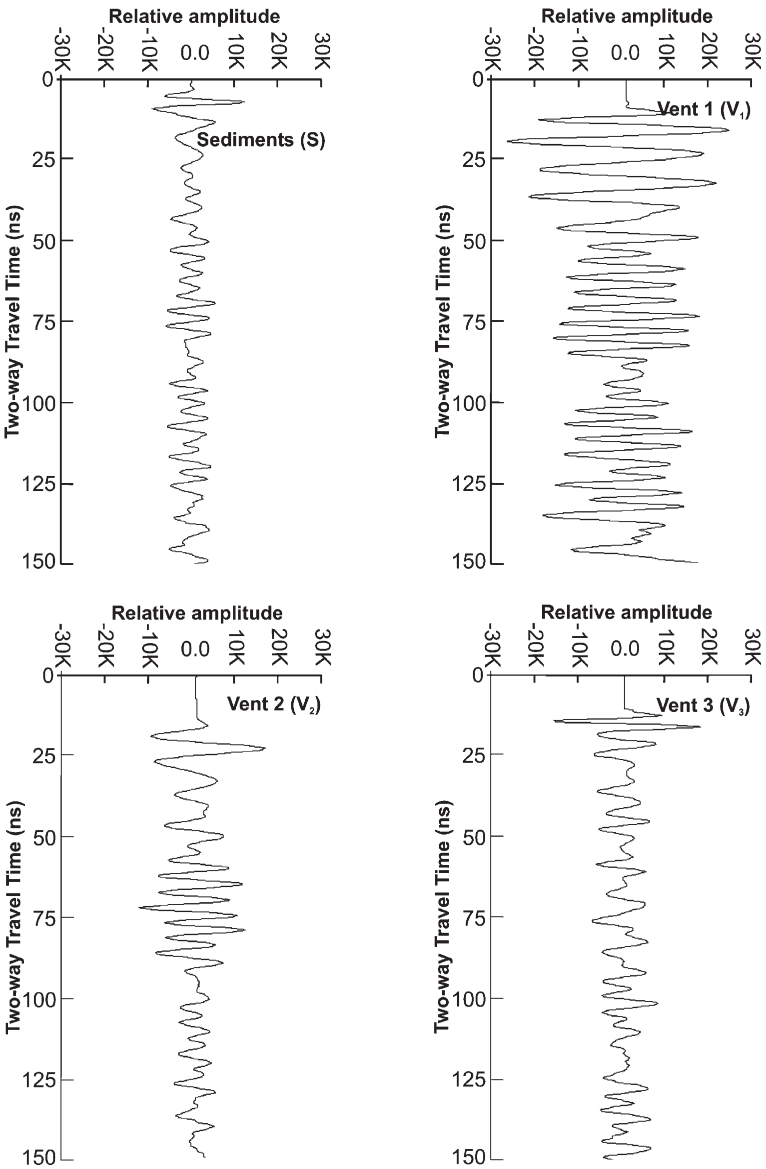

Fig. 7. One-dimensional traces showing the comparison of relative amplitudes of the host sediments (*S*) with those of the three sand vents (V_1, V_2 and V_3) identified. High amplitudes within the vents indicate their sand-dominated lithology, which is in sharp contrast with the low amplitude observed in the clay-rich host sediments. Location of the traces is shown in Fig. 6a.

concave up geometry throughout the depth of the profile conforming to the internal structure of the crater (Fig. 6a). This indicates downward settlement of the sediments into the craters after the release of pressure. All the layers appear to have preserved internal stratification, suggesting that these may not have been liquefied. The reflectors are however discontinuous below the craters which is possibly indicative of the deformation suffered by the host sediments due to sand blow activity. The deformation appear to be of both plastic as well as brittle types evidenced by sinuous reflections, suggesting the presence of convolutions (seismites) and reflection terminations indicating microfaults. The small-scale irregular sinuous reflections correspond to convolutions in thin liquefied sand layers within the clay. An irregular radar signature with sinuous form records the presence and geometry of a highly plastic layer while distinctive and homogenous radar signatures correspond to the relatively homogenous clay layers without structural features (Carreon-Freyre et al., 2003). These layers show evidence of plastic as well as brittle deformation observed as sinuous forms of the reflectors indicating plastic deformation of clay layers and abrupt truncations of some reflectors possibly indicating small-scale faults (Fig. 6a). Deformation of high plasticity compressible clay layers can occur due to their behaviour as fluid under externally forced conditions such as seismic activity (Obermeier, 1996).

7. Discussion and conclusions

The present study demonstrates the efficacy of GPR as a reliable tool for detecting internal deformation of the seismically induced liquefaction features and stratigraphic investigations of the fine-grained clay-rich sediments. The two craters visible on the surface are distinctly identifiable as separate entities in the subsurface as well. The margins of the craters are defined by contrasting radar reflection patterns, which is primarily governed by the different nature of the sediments (host sediments and crater sediments) on either side of the margins. A structureless homogenous clay dominates the lithology of the craters followed by structureless sand and large clasts of laminated sand. The clay appears to have been deposited as the water-filled craters dried out after the earthquake. Thin layers of structureless sand within the clay can possibly be attributed to the aftershocks. Such reactivation of sand blow craters due to aftershocks during a prolonged period after the main sand blow forming seismic event is well known (Sims and Garvin, 1995). The host sediments are found to be undeformed even in close vicinity of the craters, however, deformation of the host sediments below the craters is attributed to vertical settling (densification) of sediments following the release of pressure.

The craters show three centrally emplaced sand vents, one in the oblong western crater (Crater-I) and two in the circular crater (Crater-II). The vents are of roughly similar widths and continue vertically downward down the profile. The continuation of vents through the profile suggests the presence of liquefied source horizon at still deeper level. The present GPR data are not sufficient to explain the variable morphology of the sand blow craters occurring adjacent to each other. This may possibly be related to the three-dimensional structure of the sand vents. The present data suggest that the large craters in the Banni plain, related to the 2001 Bhuj earthquakes, have been formed due to liquefaction of sediments located at >6.5 m depth. This is also evident by the absence of any horizon of comparable lithology (ejected medium to coarse sand) in the host sediments.

The internal structure of the two craters studied, is the cumulative effect of seismically induced liquefaction and subsequent sediment densification. The internal geometry of the sand blow craters delineated in the present study appears to validate the model of a typical sand blow by Obermeier (1996). A typical sand blow caused by seismically induced liquefaction consists of a horizontal sheet of vented sand emanated from a steeply inclined or vertical feeder dike or duct (Lui and Li, 2001). The formation of sand blow involves upward venting of water–sediment mixture from the zone of high pore water pressure in the subsurface through an overlying cap of finer grained sediments. The first stage of liquefaction of a sediment layer involves creation of elevated pore water pressure termed as 'initial liquefaction' which may be followed by combination of elevated pore pressure with large loss of strength referred to as complete liquefaction (Obermeier, 1996). The liquefaction is followed by vertical settlement caused by 'sediment densification', which progresses bottom upwards (Scott, 1986) after water is expelled from the sediments creating a crater mostly of circular outline on the surface. Original stratification may be only partially disturbed in layers which have suffered only initial liquefaction (Obermeier, 1996).

We infer that the fine grained clay-rich sediments of the Banni plain acted as a 'finer grained cap' above the liquefiable sand horizon at >6.5 m depth. The finer grained cap suffered only initial liquefaction as evidenced by the well preserved stratification of the sand-rich layers within the sand blow craters. This may be attributed to the presence significant amounts of clay in the Holocene sediments of the Banni plain and Great Rann. Liquefaction is unusual in sediments containing more that 15% clay as it greatly diminishes the ability of the sediments to liquefy and flow (Seed et al., 1983). We visualise a similar scenario for the extensive liquefaction caused during earlier large earthquakes, for example, the Allahbund earthquake, presumed to have produced a 80 km long and 5–6 m high surface rupture in the northern part of the Great Rann (Mac Murdo, 1824). It would be interesting to locate and study the liquefaction features of previous large earthquakes in the area and compare them with the results of the present study. This would enable understanding phenomena of repeated liquefaction in the Banni Plain and Great Rann of Kachchh and their relationship with distance from earthquake epicenters.

Acknowledgements

The authors are grateful to the Department of Science and Technology, New Delhi, India (Project No. DST/23 (324)/SU/2001), for the financial support to carry out the present study. Constructive reviews by two anonymous referees are gratefully acknowledged. We greatly appreciate the help and advice received from Dr. Adrian Neal, Dr. Lawrence B. Conyers and Dr. Andreas Kathage in our study.

References

Bano, M., Marquis, G., Niviere, B., Maurin, J.C., Cushing, M., 2000. Investigating alluvial and tectonic features with Ground Penetrating Radar and analyzing diffraction patterns. Journal of Applied Geophysics 43, 33–41.

Bridge, J.S., Collier, R.E.L., Alexander, J., 1998. Large scale structure of Calamas river deposits (Nebraska, USA) revealed using Ground Penetrating Radar. Sedimentology 45, 977–986.

Busby, J.P., Merritt, J.W., 1999. Quaternary deformation mapping with Ground Penetrating Radar. Journal of Applied Geophysics 41, 75–91.

Carreon-Freyre, D., Cerca, M., Hernandez-Marin, M., 2003. Correlation of near-surface stratigraphy and physical properties of clayey sediments from Chalco Basin, Mexico, using Ground Penetrating Radar. Journal of Applied Geophysics 53, 121–136.

Chow, J., Angelier, J., Hua, J.-J., Lee, J.-C., Sun, R., 2001. Palaeoseismic events and active faulting: from Ground Penetrating Radarand high resolution seismic reflection profiles across the Chihshary fault, Eastern Taiwan. Tectonophysics 333, 241–259.

Davis, J.L., Annan, A.P., 1989. Ground penetration radar for high resolution mapping of soil and rock stratigraphy. Geophysical Prospecting 37, 531–551.

Feilding, C.R., Alexander, J., McDonald, R., 1999. Sedimentary facies from Ground Penetrating Radar surveys of the modern, Upper Burdekin River of North Queensland, Australia: consequences of extreme discharge fluctuations. International Association of Sedimentology, Special Publications 28, 347–362.

Gawthrope, R.L., Collier, R.E.L., Alexander, J., Bridge, J.S., Leeder, M.R., 1993. Ground Penetrating Radar: application of sandbody geometry and heterogeneity studies. In: North, C.J., Prosser, D.J. (Eds.), Characterization of Fluvial and Aeolian Reservoirs. Special Publication-Geological Society of London, vol. 73, pp. 421–432.

Glennie, K.W., Evans, G., 1976. A reconnaissance of the Great Rann of Kachchh, India. Sedimentology 23, 625–647.

Jol, H.M., 1995. Ground Penetrating Radar antennae frequencies and transmitter powers compared for penetration depth, resolution and reflection continuity. Geophysical Prospecting 43, 693–709.

Jol, H.M., Bristow, C.S., 2003. GPR in sediments: advice on data collection, basic processing and interpretation, a good practice guide. In: Bristow, C.S., Jol, H.M. (Eds.), Ground Penetrating Radar in Sediments. Special Publication-Geological Society of London, vol. 211, pp. 9–27.

Jol, H.M., Smith, D.G., 1991. Ground Penetrating Radar of northern lacustrine deltas. Canadian Journal of Earth Sciences 28, 1939–1947.

Jol, H.M., Smith, D.G., Meyers, R.A., 1996. Digital Ground Penetrating Radar (GPR): an improved and very effective geophysical tool for studying modern coastal barriers (examples for the Atlantic, Gulf and Pacific coasts, U.S.A.). Journal of Coastal Research 12, 960–968.

Kar, A., 1995. Geomorphology of the Western India. Memoir-Geological Society of India 32, 168–190.

Lui, L., Li, Y., 2001. Identification of liquefaction and deformation features using Ground Penetrating Radar in the New Madrid Seismic Zone, USA. Journal of Applied Geophysics 47, 199–215.

Mac Murdo, J., 1824. Papers relating to the earthquake which occurred in India in 1819. Philosophical Magazine 63, 105–177.

Maurya, D.M., Patidar, A.K., Mulchandani, N., Goyal, B., Thakkar, M.G., Bhandari, S., Vaid, S.I., Bhatt, N.P., Chamyal, L.S., 2005. Need for initiating Ground Penetrating Radar studies along active faults in India: an example from Kachchh. Current Science 88, 231–240.

McCalpin, J.P., Thakkar, M.G., 2003. 2001 Bhuj–Kachchh earthquake: surface faulting and its relation with neotectonics and regional structures, Gujarat, Western India. Annals of Geophysics 46, 937–956.

Neal, A., 2004. Ground-penetrating radar and its use in sedimentology: principles, problems and progress. Earth-Science Reviews 66, 261–330.

Obermeier, S.F., 1996. Using liquefaction-induced features for paleoseismic analysis. In: McCalpin, J.P. (Ed.), Paleoseismology. Academic Press, London, pp. 331–396.

Quittmeyer, R.C., Jacob, K.H., 1979. Historical and Modern seismicity of Pakistan, Afghanistan, north-western India, and south-eastern Iran. Bulletin of the Seismological Society of America 69, 773–823.

Rajendran, K., Rajendran, C.P., Thakkar, M.G., Tuttle, M.P., 2001. The 2001 Kutch (Bhuj) earthquake: coseismic features and their significance. Current Science 80, 1397–1405.

Rajendran, K., Rajendran, C.P., Thakkar, M.G., Gartia, R.K., 2002. Sand blows from the 2001 Bhuj earthquake reveal clues on past seismicity. Current Science 83, 603–610.

Roy, B., Merh, S.S., 1981. The Great Rann of Kutch—an intriguing Quaternary terrain. Recent Research in Geology. Hindustan Publishing Corporation, India, pp. 100–108.

Saarenketo, T., 1998. Electrical properties of water in clay and silty soil. Journal of Applied Geophysics 40, 73–88.

Schweig, E., Gomberg, J., Petersen, M., Ellis, M., Bodin, P., Mayrose, L., Rastogi, B.K., 2003. The Mw 7.7 Bhuj Earthquake: global lessons for earthquake hazard in intra-plate regions. Journal of the Geological Society of India 61, 277–282.

Scott, R.F., 1986. Solidification and consolidation of a liquefied sand column. Soils and Foundations. Japanese Society of Soil Mechanics Foundation Engineers 26, 23–31.

Seed, H.B., Idriss, I.M., Arango, I., 1983. Evaluation of liquefaction potential using field performance data. Journal of Geotechnical Engineering, American Society of Civil Engineers 109, 458–482.

Sims, J.D., Garvin, C.D., 1995. Recurrent liquefaction induced by the 1989 Loma Preita earthquake and 1990 and 1991 aftershocks: implications for palaeoseismicity studies. Bulletin of the Seismological Society of America 85, 51–65.

Srivastava, P.K., 1971. Recent sediments of the Ranns of Kutch. Journal of the Geological Society of India 12, 392–395.

Thakkar, M.G., Goyal, B., 2004. On the relation between magnitude and liquefaction dimension at the Epicentral zone of 2001 Bhuj Earthquake. Current Science 67, 811–817.

Tuttle, M.P., Hengesh, J., Tucker, K.B., Lettis, W., Deaton, S.L., Frost, J.D., 2002. Observations and comparisons of liquefaction features and related effects induced by the Bhuj earthquake. Earthquake Spectra 18, 79–100.

Van Dam, R.L., Schlager, W., 2000. Identifying causes of ground-penetrating radar reflections using time-domain reflectometry and sedimentological analyses. Sedimentology 47, 435–449.